

Determination of the $[\text{Pt}(\text{NH}_3)_5\text{Cl}]\text{Br}_3$ crystal structure from X-ray powder diffraction data using multi-population genetic algorithm

A. N. Zaloga,^{a)} I. S. Yakimov, and P. S. Dubinin
Siberian Federal University, Krasnoyarsk, Russia

(Received 15 September 2016; accepted 23 January 2017)

The paper describes an approach for automated crystal structure solution from powder diffraction data using the multi-population genetic algorithm (MPGA). The advantage of using co-evolution with the best individual exchange, compared with the using of the evolution with a single genetic algorithm without interpopulation exchange, is shown. As an example, the paper describes the use of MPGA for solving the $[\text{Pt}(\text{NH}_3)_5\text{Cl}]\text{Br}_3$ crystal structure, having the tetragonal $I4_1/a$ space group [$a = 17.2587(5) \text{ \AA}$, $c = 15.1164(3) \text{ \AA}$, $Z = 16$, unit-cell volume $V = 4502.61(10) \text{ \AA}^3$]. The MPGA convergence charts and the atomic positions distribution maps of the MPGA populations are given. The description of the final structure solution is also shown. © 2017 International Centre for Diffraction Data.

[doi:10.1017/S0885715617000197]

Key words: X-ray powder diffraction, crystal structure analysis in direct space, genetic algorithms, full-profile analysis, Rietveld method

I. INTRODUCTION

Direct space methods for crystal structure solution from powder diffraction data, including the Monte Carlo method (Kariuki *et al.*, 1996; Andreev *et al.*, 1997), genetic algorithms (GAs) (Kariuki *et al.*, 1997; Shankland *et al.*, 1997), and simulated annealing (Andreev and Bruce, 1988; David *et al.*, 1998), began their development with the appearance of high-speed computers at the beginning of 1990s. Nowadays, programs using the simulated annealing method, such as FOX (Favre-Nicolin and Černý, 2002), DASH (David *et al.*, 2006), and TOPAS (Whitfield *et al.*, 2010), are widely applied. GAs are implemented in the known EAGER (Harris *et al.*, 1998), GEST (Feng and Dong, 2007), and MAUD (Lutterotti and Bortolotti, 2003) programs. The essence of GA is the modeling of natural biological selection operations: pairwise crossing, mutation, and selection of the best trial structural models for getting new advanced generations.

According to Le Bail and Cranswick (2009), the crystal structures of over 200 new substances are annually solved by methods of global optimization in direct space. A common problem of these methods is a deterioration in the convergence along with an increase in the complexity of determined structures because of a non-linearly growing probability of GA and stagnation in the numerous local minima of the R -factor hypersurface. Therefore, in practice their use is limited by the number of degrees of freedom to be varied (usually no more than 30–50). Simulated annealing techniques are the most common and easy to use amongst the methods of global optimization in the direct space. Shankland *et al.* (2013) point out that the principal disadvantage in the GA implementation is the need to set numerous parameters that regulate the evolution processes.

With the increase in the number of multi-core computers and clusters, parallel computing becomes more popular. For example, related versions of FOX.Grid (Rohlíček *et al.*, 2010), GDASH (Griffin *et al.*, 2009a), and MDASH (Griffin *et al.*, 2009b) software have been developed. Meredig and Wolverton (2013) describe a new hybrid approach for the automated crystal structure solution, which combines the application of GAs for the crystal structure algorithmic optimization from experimental diffraction data with the calculation of structural models from the first-principles density functional theory energies. Articles dedicated to the development of different parallel GA models for supercomputing clusters and application of distributed computing in a number of other science and technology fields, are being published increasingly (Falahiazar *et al.*, 2012; Kurose *et al.*, 2012; To and Elati, 2013; Nalepa and Blocho, 2014; Ozkan *et al.*, 2015).

The first version of the parallel GA for crystal structure solution was proposed by Habershon *et al.* (2003). This version is based on the successfully used single-population GA (Albesa-Jové *et al.*, 2004), which is complemented with a direct exchange of random structural models among different GA populations. However, this approach has not been sufficiently developed so far. At the same time, GAs have two essential advantages. Firstly, they simultaneously execute the evolution of the whole set (population) of trial structural models, i.e. explore in parallel a wide region of the structural parameters space. Secondly, the parallel GA is much better suited for implementation on supercomputing clusters than in a single one. This creates the possibility of using the full power of parallel computing for structural analysis (Habershon *et al.*, 2003). The multi-population approach could help to solve more complex structures, but it has not almost been investigated so far.

We present a multi-population parallel GA, which implements co-evolution of independent GA processes on computational cores of multicore PC or cluster. Co-evolution is

^{a)}Author to whom correspondence should be addressed. Electronic mail: zaloga@yandex.ru

performed by accumulating the best trial structural models on the managing core and then selectively transmitting them into populations on the working cores. Such approach contributes to getting out from local minima of the *R*-factor hypersurface, accelerates the accumulation of correct atomic positions in the populations and increases the probability of GA convergence when more complex structures (Burakov *et al.*, 2015) are managed.

II. EXPERIMENTAL

A. Features of MPGA

The design and the current features of MPGA are described in more detail by Burakov *et al.* (2015). Below we present a general description of its original features. The main ones are:

- (1) Appointing of penalties to a structure:
 - if the distance among atoms is less than a minimum value,
 - if the number of interatomic bonds is different from the theoretical one.
- (2) Working with the molecular fragments and restricting of distances and angles within the fragments.
- (3) Automatically putting the atoms on the symmetry elements if near to them.
- (4) Working with multi-phase samples.
- (5) Providing built-in tools for the convergence process analysis: convergence chart for each core, 3D crystal structure, atoms distribution maps at each generation.
- (6) Being based on the FOX/ObjCryst++ library (Favre-Nicolin and Cerný, 2002).

Figure 1 shows the flow-chart of MPGA. Green color indicates working cores, which execute individual GA processes. Yellow color indicates a managing core, where the accumulation of the best structures and the control of their distribution to the working cores is carried out.

From this flow-chart the factors improving the MPGA convergence can be seen:

- (1) the execution of independent parallel processes with different settings on working cores;

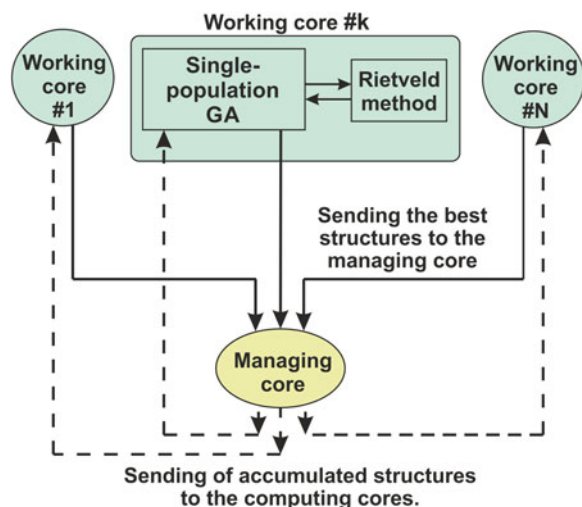


Figure 1. (Color online) The flowchart of MPGA.

- (2) the refinement of the best structures by the Rietveld method;
- (3) the co-evolution involving accumulation and a managed exchange of the best solutions among the GA processes.

B. Analysis of the MPGA effectiveness increasing the amount of involved resources

Comparative tests of MPGA with different amount of involved resources were conducted over several known crystal structures. Results are shown in Table I. It demonstrates that the structure determination on four-core PC is two to three times as reliable as for the single-population GA, while for supercomputer cluster it is two to fourtimes as reliable as for four-core PC. The table has only one column “Time per run”, because in all modes the number of parallel processes was different, while the number of generations and the number of individuals in each process was the same.

C. Determination of the crystal structure of $[\text{Pt}(\text{NH}_3)_5\text{Cl}]\text{Br}_3$ using MPGA

1. Description of the input data for the determination of the crystal structure

The unknown crystal structure of $[\text{Pt}(\text{NH}_3)_5\text{Cl}]\text{Br}_3$, synthesized from standard chemical reagents with a purity not less than “chemically pure—analytically pure”, has been chosen to be solved. Synthesis of $[\text{Pt}(\text{NH}_3)_5\text{Cl}]\text{Br}_3$ was made as follows. The complex compound $[\text{Pt}(\text{NH}_3)_5\text{Cl}]\text{Cl}_3 \times \text{H}_2\text{O}$, obtained in accordance with Chernyaev (1964), was dissolved in a minimum amount of water at 30–40 °C, then a concentrated solution of potassium bromide with a molar ratio Pt : Br = 1 : (3–4) was added. The formed precipitate was filtered, washed with water and ethanol and subsequently dried on a filter. The X-ray powder diffraction pattern was recorded in the reflection geometry on a PANalytical X’Pert PRO diffractometer with a PIXcel detector (CoK α radiation, 2θ scan range 6°–110°). The indexing of the diffraction pattern and the determination of the space group symmetry were carried out by the EXPO program (Altomare *et al.*, 2004). As a result, the following crystallographic characteristics were determined: space group $I4_1/a$, unit-cell parameters $a = 17.2587(5)$ Å; $c = 15.1164(3)$ Å, $V = 4502.61(10)$ Å³, $Z = 16$, with $M_{20} = 20$ and $F_{20} = 38$. The conformity of all the experimental diffraction peak positions to those calculated from the crystal lattice parameters confirmed the purity of the chemical synthesis.

The profile parameters of the diffraction pattern and the target value of the profile *R*-factor equal to 5.49% were determined using the Le Bail method. Restrictions on the interatomic distances were imposed according to the statistics of the interatomic distances distribution, which has been calculated by Diamond program (Pennington, 1999) using structures having a similar composition.

The required parameters for solving this structure by MPGA were the locations of three Br atoms and the a priori knowledge of the structural fragment of PtN_5Cl (its orientation was described by quaternion consisting of four elements) in the unit cell. The hydrogen atoms were not taken into account at this stage, whereas the parameters of the atomic isotropic thermal oscillations were taken from structures of similar composition. The total number of degrees of freedom for this structure is 16.

TABLE I. The MPGA performances and efficiency investigated on known structures.

Tested structure	Degrees of freedom	Frequency of the single-population GA convergence (%)	Frequency of the MPGA convergence on a PC (four cores) (%)	Frequency of the MPGA convergence on a cluster (24 cores) (%)	Average time per run, minutes
Ba ₂ CrO ₄ (Mattausch and Müller-Buschbaum, 1974)	21	70	100	100	2
K ₄ SnO ₄ (Marchand <i>et al.</i> , 1975)	27	33	76	100	2
K ₂ PbO ₂ (Martens and Hoppe, 1978)	30	27	64	95	3
Ca ₂ Al ₃ O ₆ F (Xia <i>et al.</i> , 2014)	25	8	28	44	15
CaC ₄ H ₄ O ₆ · 4H ₂ O (Le Bail and Cranswick, 2009)	22	0	30	60	8
Er ₁₀ W ₂ O ₂₁ (Bevan <i>et al.</i> , 1982)	54	0	10	40	23
[Pt(NH ₃) ₅ Cl]Br ₃	16	15	35	70	12

The crystal structure determination was performed using the MPGA software on a computer equipped with an Intel i7–3770 processor having eight processing threads. Seven of them were involved in the evolutionary search of the crystal structure in independent populations and one thread managed the accumulation of the best structural models from the generated populations and the exchange between populations (Zaloga *et al.*, 2014). The MPGA version providing real-coded atomic coordinates and the periodical local optimization of the best structural models by local search (LS) of the Rietveld method (Burakov *et al.*, 2015) was used. The evolutionary search of the crystal structure was performed automatically after the MPGA launch, and the process was visually controlled with convergence charts, charts of atomic positions distribution in the populations, and comparative charts between the experimental powder pattern and that one obtained from the best structural model in a current generation. It should be mentioned that the presetting of the search parameters for the MPGA operation is required because their quality affect the probability of GA to converge to the correct structure. This was achieved by an empirical selection from the parameters used in the MPGA launches for searching the known crystal structures of [Pd(NH₃)₄](C₂O₄) and [Pt(NH₃)₂(C₂O₄)], which compositions are similar to the investigated structure's one.

2. MPGA convergence during the structure determination of [Pt(NH₃)₅Cl]Br₃

Figure 2 shows the graph of the MPGA convergence for the [Pt(NH₃)₅Cl]Br₃ structure determination. The combination

of the reported diagrams allows the control and the analysis of the convergence process.

It can be seen from Figure 2 that by the 40th generation of the evolution process, the fitness value of 15% rel. was reached and the structure had been essentially formed. However, it was not yet fully correct, because the interatomic distances were beyond the limits (a penalty level for this trial structure was about 15% of a fitness value). By the hundredth generation the penalty had disappeared, all the interatomic distances had become correct and the fitness value had coincided with the *R*-factor value. Next, the *R*-factor was gradually reduced from 13.5 to 12% rel., mainly because of the refinement of the PtN₅Cl fragment's orientation, and by the 180th generation the convergence had been completed. Wherein, the best structural models were gradually spread over the populations on the working cores (the green line is decreasing). It should be noted that almost all sharp declines of the fitness function occurred because of a local optimization of the structural models (the red line becomes coincident with the black one).

A new visualizer was developed to better understanding the GA convergence processes in populations in the working cores. It allows visualizing the projection of the atomic positions at chosen basic planes of the unit cell (e.g., *ac*) for all structural models in a population at a chosen generation. It is possible to specify the atomic coordinates of a known structure to compare with, and these positions will be marked with colored crosses (+). Thus, the visualizer allows us to scroll and compare in real time the distributions of atoms in different populations at different evolutionary generations and compares them with the working cores convergence charts, etc.

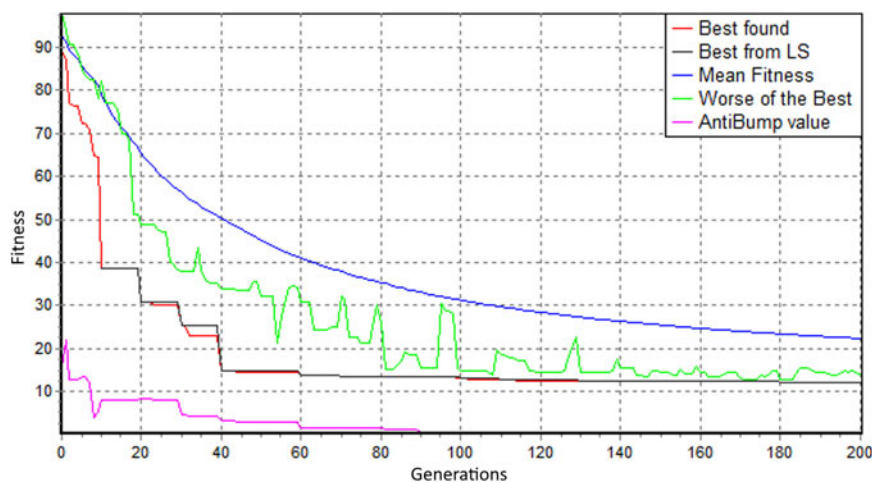


Figure 2. (Color online) MPGA convergence graph for the search of [Pt(NH₃)₅Cl]Br₃ structure. The X-axis is the number of generations in the population (the number zero is the initial random generation of all populations); the Y-axis is the fitness function value (*R*-factor plus penalties for violation of the structural limitations) of the best structural model selected from the accumulated structures at the control core. The red line is the fitness value for the best found structural models. The black line is the best fitness value obtained after the refinement of the best structural model by the LS method (it has a stepped appearance when the LS execution mode sets to once every few generations). The purple line is the contribution of penalties to the fitness function value. The blue line is the average fitness value of the structural solutions accumulated on the managing core. The green line is the fitness value of the worst, among the best, solutions on the working cores.

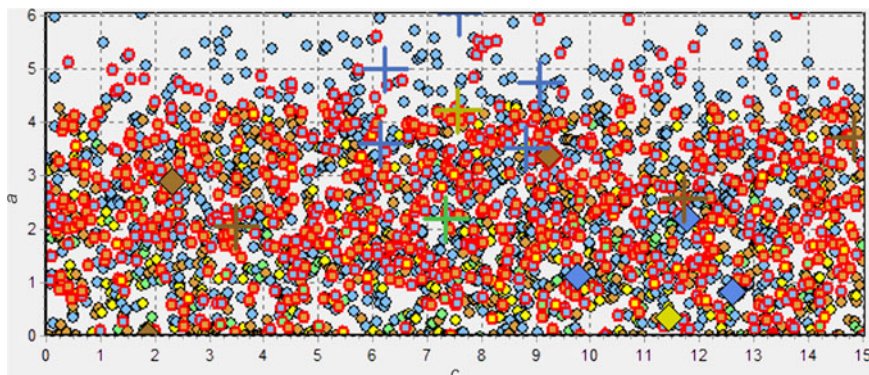


Figure 3. (Color online) First generation. Completely random structures. R_{wp} value of the best solution = 84.36%. The X-axis is the direction c (Å) in the unit cell; the Y-axis is the direction a (Å) in the unit cell.

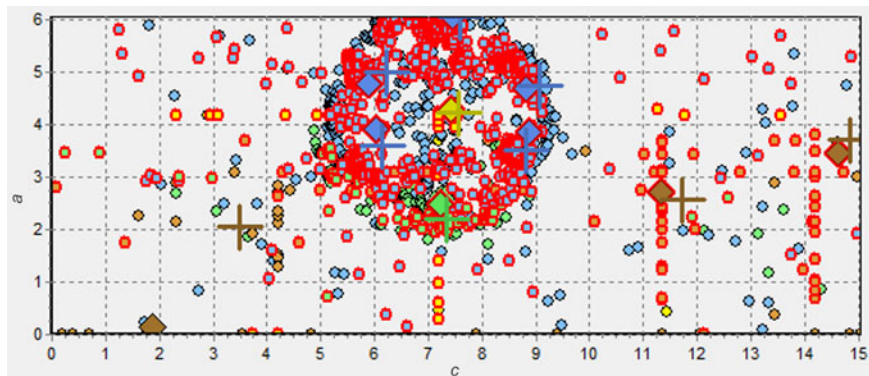


Figure 4. (Color online) 21st generation. 70% of the atoms are close to the correct positions. R_{wp} value of the best solution = 40.78%. The X-axis is the direction c (Å) in the unit cell; the Y-axis is the direction a (Å) in the unit cell.

In particular, this tool is very useful to study the MPGA convergence on the test crystal structures.

To illustrate the MPGA convergence process, atomic positions distribution maps for the $[\text{Pt}(\text{NH}_3)_5\text{Cl}]\text{Br}_3$ search are reported in Figures 3–5. The projection of an independent part of the cell on the ac -plane is shown. Crosses (+) indicate correct positions; diamonds indicate the positions of the best structure's atoms; circles indicate the other atoms. Pt atoms are shown in yellow, N in blue, Cl in green, and Br in brown.

The pictures demonstrate how the atomic positions in a population of structure models evolve from randomly generated (Figure 3) to the correct positions (shown with the crosses (+)), identified from a full-profile refinement of the best structural model.

3. Refinement of the crystal structure

The structural model obtained from the MPGA had been refined by the DDM full-profile analysis software (Solovyov,

2004) involving the thermal oscillation parameters of the atoms. The obtained R -factor value of 7.64% was higher than the target value by 2.15%. Next, the positions of the hydrogen atoms, which are chemically bonded with the nitrogen atoms in NH_3 groups (taken from similar structures in the ICSD database), were added to the structure and the DDM refinement was repeated. Hydrogens were rigidly attached to the nitrogen so that just the positions of the NH_3 groups were refined. As result, the profile R -factor had been reduced to 6.89%. However, it still was by 1.9% higher than the target value and the values of the isotropic thermal oscillation coefficients of Br atoms (especially Br3) were too high. Thus, it was concluded that a number of Br atoms is statistically replaced with lighter Cl atoms. To take this into account, three Cl atoms were added to the structure in positions of Br atoms and their occupancy factors were functionally associated with the occupancy factors of the appropriate Br atoms. Figure 6 shows DDM settings for the refinement of a non-stoichiometric variant of the $[\text{Pt}(\text{NH}_3)_5\text{Cl}]\text{Br}_{3-x}\text{Cl}_x$ structure.

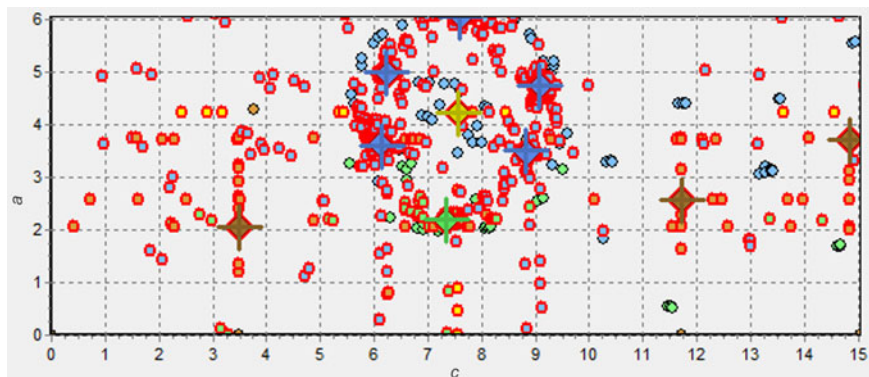


Figure 5. (Color online) 200th generation. R_{wp} value of the best solution = 11.13%. The X-axis is the direction c (Å) in the unit cell; the Y-axis is the direction a (Å) in the unit cell.

Name	Type	X	Y	Z	N	Biso	Dist	Aniso
Pt	Pt+4	0.245790	0.268408	0.502131	16.00000	1.586708	2.350	
Br1	Br-1	0.125618	0.282629	0.231992	14.36683	2.400329	0.000	
Br2	Br-1	0.283708	0.527841	0.485314	14.76441	2.770951	0.000	
Br3	Br-1	0.149428	0.308202	0.766927	9.44091	2.356355	0.000	
Cl1	Cl-1	0.125618	0.282629	0.231992	1.63317	2.400329	0.000	
Cl2	Cl-1	0.283708	0.527841	0.485314	1.23559	2.770951	0.000	
Cl3	Cl-1	0.149428	0.308202	0.766927	6.55909	2.356355	0.000	
Cl4	Cl-1	0.126060	0.325580	0.493591	16.00000	2.700477	0.000	
N1	N	0.353691	0.216381	0.519378	16.00000	1.223119	0.000	
N2	N	0.213213	0.190200	0.406011	16.00000	1.223119	0.000	
N3	N	0.279471	0.350369	0.594746	16.00000	1.223119	0.000	
N4	N	0.200655	0.195169	0.596677	16.00000	1.223119	0.000	
N5	N	0.287456	0.342279	0.408421	16.00000	1.223119	0.000	
H11	H	0.392396	0.243787	0.487459	16.00000	3.000000	0.000	
H12	H	0.366796	0.152387	0.580359	16.00000	3.000000	0.000	
H13	H	0.350396	0.164787	0.497559	16.00000	3.000000	0.000	
H21	H	0.254513	0.155100	0.394411	16.00000	3.000000	0.000	
H22	H	0.169713	0.162300	0.427511	16.00000	3.000000	0.000	
H23	H	0.199513	0.216300	0.352911	16.00000	3.000000	0.000	
H31	H	0.331271	0.340869	0.612846	16.00000	3.000000	0.000	
H32	H	0.245971	0.346569	0.644346	16.00000	3.000000	0.000	
H33	H	0.275971	0.400969	0.570146	16.00000	3.000000	0.000	
H41	H	0.147655	0.208069	0.604377	16.00000	3.000000	0.000	
H42	H	0.227655	0.202969	0.650777	16.00000	3.000000	0.000	
H43	H	0.204955	0.142369	0.579577	16.00000	3.000000	0.000	
H51	H	0.247356	0.375879	0.388921	16.00000	3.000000	0.000	
H52	H	0.328056	0.371879	0.434021	16.00000	3.000000	0.000	
H53	H	0.307056	0.313779	0.359521	16.00000	3.000000	0.000	

Figure 6. (Color online) Settings of the DDM program for the refinement of non-stoichiometric $[\text{Pt}(\text{NH}_3)_5\text{Cl}]\text{Br}_{3-x}\text{Cl}_x$ structure, the refining parameters marked by buttons: independent, by green; functionally connected, by orange (numbers on the buttons show connection number).

III. RESULTS AND DISCUSSION

The probability that the atomic coordinate will be randomly generated in neighborhood of its correct position (no more than ~ 0.03 of the length of the unit-cell axis from the correct position; on Figures 3–5 it is the radius of crosses) is about $1/33$. It is experimentally shown by Yakimov *et al.* (2013) that a structural model having atoms quite precisely localized can be effectively refined by the LS method (at least, when the lengths of the unit-cell axes are up to 10–15 Å). The initial population of even 50 structural models contains in average one or two such coordinates for each atom (in different models). The MPGA convergence is produced by an evolutionary accumulation of “good” coordinates in a population (it goes step by step from heavy atoms to light atoms) because of successful crossings and the LS minimization.

It is because the R -factor has statistical sensitivity to determining the correct set of the heavy atom atomic coordinates, while the other lighter atoms are distributed randomly (Yakimov *et al.*, 2013). In addition, it is complemented by the exception of chemically incorrect structural models (by adding a penalty to the R -factor value).

The final refinement of the structural model found by DDM resulted in a profile R -factor value of 5.64%, which corresponded well with the target value of 5.49%. Figure 7 shows the comparison between the experimental and the calculated powder diffraction pattern, this last from the refined structure. The atomic coordinates, atomic isotropic thermal parameters and the occupancy coefficients are shown in Table II. The calculated chemical formula of the compound (according to Table II) is $[\text{Pt}(\text{NH}_3)_5\text{Cl}]\text{Br}_{2.4}\text{Cl}_{0.6}$.

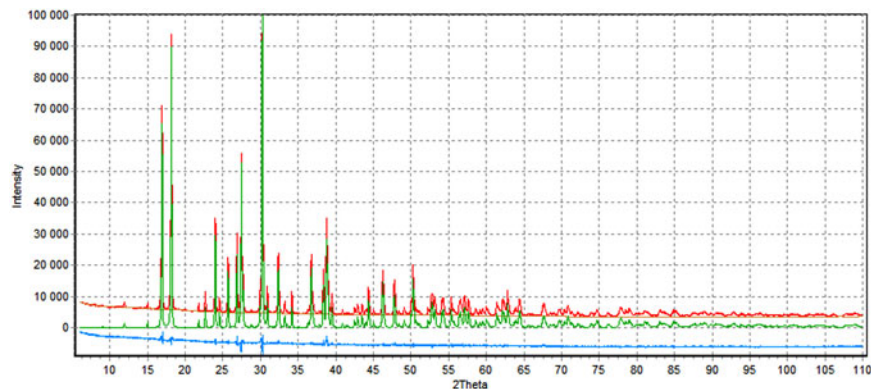


Figure 7. (Color online) Comparison of the experimental diffraction pattern (the red line) and the calculated one (the green line) obtained after the final refinement by DDM, for the $[\text{Pt}(\text{NH}_3)_5\text{Cl}]\text{Br}_{2.4}\text{Cl}_{0.6}$ compound; the blue line represents the difference profile; the R -factor value is 5.637%. The X -axis is the scattering angle 2θ ; the Y -axis is the scattering intensity.

TABLE II. Fractional atomic coordinates, isotropic displacement parameters (\AA^2) and occupancy for $[\text{Pt}(\text{NH}_3)_5\text{Cl}]\text{Br}_{2.4}\text{Cl}_{0.6}$ crystal structure.

Atom	X	Y	Z	U_{iso}	Occup.
Pt	0.24579 (10)	0.26841 (7)	0.50209 (15)	0.015 (6)	1.0
Br1	0.12571 (23)	0.28267 (24)	0.23195 (38)	0.026 (6)	0.896 (12)
Cl1	0.12571 (23)	0.28267 (24)	0.23195 (38)	0.026 (6)	0.104 (12)
Br2	0.28375 (21)	0.52788 (18)	0.48527 (24)	0.030 (6)	0.921 (9)
Cl2	0.28375 (21)	0.52788 (18)	0.48527 (24)	0.030 (6)	0.079 (9)
Br3	0.14937 (29)	0.30820 (26)	0.76687 (42)	0.025 (6)	0.587 (12)
Cl3	0.14937 (29)	0.30820 (26)	0.76687 (42)	0.025 (6)	0.413 (12)
Cl4	0.1262 (5)	0.32560 (38)	0.4936 (9)	0.030 (6)	1.0
N1	0.3534 (10)	0.2167 (11)	0.5192 (16)	0.011 (7)	1.0
N2	0.2130 (17)	0.1903 (12)	0.4063 (12)	0.011 (7)	1.0
N3	0.2792 (15)	0.3501 (13)	0.5946 (13)	0.011 (7)	1.0
N4	0.2008 (15)	0.1954 (13)	0.5960 (12)	0.011 (7)	1.0
N5	0.2872 (14)	0.3424 (12)	0.4083 (13)	0.011 (7)	1.0
H11	0.39 (1)	0.24 (1)	0.49 (1)	0.038	1.0
H12	0.37	0.22	0.58	0.038	1.0
H13	0.35	0.17	0.49	0.038	1.0
H21	0.25	0.16	0.34	0.038	1.0
H22	0.17	0.16	0.43	0.038	1.0
H23	0.20	0.22	0.35	0.038	1.0
H31	0.33	0.34	0.61	0.038	1.0
H32	0.25	0.35	0.64	0.038	1.0
H33	0.28	0.40	0.57	0.038	1.0
H41	0.15	0.21	0.60	0.038	1.0
H42	0.23	0.20	0.65	0.038	1.0
H43	0.21	0.14	0.58	0.038	1.0
H51	0.25	0.38	0.39	0.038	1.0
H52	0.33	0.37	0.43	0.038	1.0
H53	0.30	0.31	0.36	0.0380	1.0

The scheme of atoms localization in the $[\text{Pt}(\text{NH}_3)_5\text{Cl}]\text{Br}_{2.4}\text{Cl}_{0.6}$ crystal structure is shown in Figures 8 and 9.

The crystal structure is built with complex $[\text{Pt}(\text{NH}_3)_5\text{Cl}]^{3+}$ cations and three crystallographically independent Br^- anions. All the atoms are located in general positions. because of the presence of the chlorine atom, the complex cation shapes are

distorted octahedra having the following bond lengths: Pt–Cl4 = 2291 \AA ; Pt–N1 = 2077 \AA ; Pt–N2 = 2058 \AA ; Pt–N3 = 2067 \AA ; Pt–N4 = 2051 \AA ; Pt–N5 = 2038 \AA . The N1 and Cl4 atoms are located at the vertices of the octahedron, while the other four nitrogen atoms lie at its base. The N–Pt–N angles in the octahedron base deviate from the right ones and range

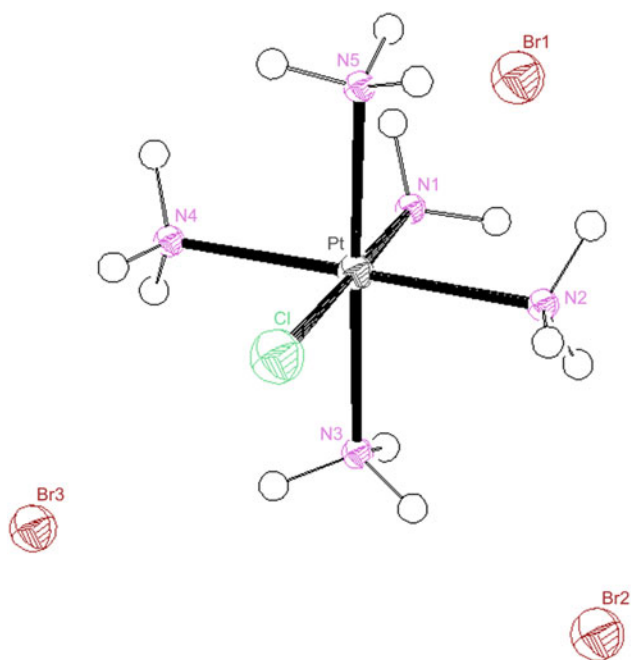


Figure 8. (Color online) The complex cation $[\text{Pt}(\text{NH}_3)_5\text{Cl}]^{3+}$ surrounded by three independent Br^- anions in the $[\text{Pt}(\text{NH}_3)_5\text{Cl}]\text{Br}_{2.4}\text{Cl}_{0.6}$ crystal structure.

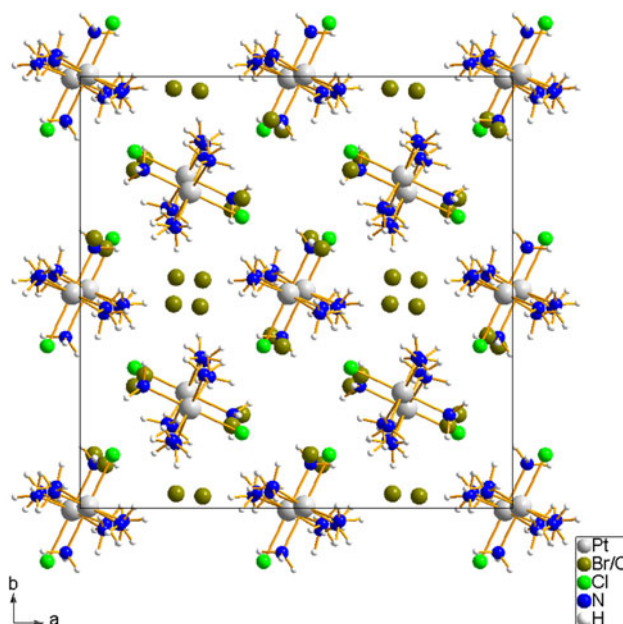


Figure 9. (Color online) The projection of the $[\text{Pt}(\text{NH}_3)_5\text{Cl}]\text{Br}_{2.4}\text{Cl}_{0.6}$ crystal structure on the ab -plane of the crystal lattice.

from 86.9 to 93.2°. The angle among the atoms at the vertices of the N1–Pt–Cl4 octahedron is 176°. These bond lengths agree well with the interatomic distances in similar structures. A good correspondence between interatomic bond lengths and their statistical distribution in similar structures and a low value of the profile *R*-factor indicate the adequacy of the found crystal structure. A check by the online IUCr CheckCIF/PLATON service (Spek, 2003) confirmed the structure correctness.

IV. CONCLUSION

The MPGA software, implementing a multi-population GA and using parallel computing on multi-core PCs and supercomputer clusters, was developed. A further development of MPGA for solving more complex structures has been planned.

It was shown that the increase in the number of processing cores allows the structure solution of more complex structures. The structure determination on four-core PC was two to three times as reliable as for the single-population GA, while for supercomputer cluster it was two to four times as reliable as for four-core PC.

The crystal structure of the complex compound [Pt(NH₃)₅Cl]Br₃ was determined by multi-population GA, and then refined with the localization of the hydrogen atoms by DDM software. Non-stoichiometry of the synthesized compound was determined. The positions of each of the Br anions are statistically partially occupied by Cl anions. The overall chemical formula is [Pt(NH₃)₅Cl]Br_{2.4}Cl_{0.6}.

SUPPLEMENTARY MATERIAL

The supplementary material for this article can be found at <https://doi.org/10.1017/S0885715617000197>

ACKNOWLEDGEMENTS

The reported study was funded by Russian Foundation for Basic Research, Government of Krasnoyarsk Territory, Krasnoyarsk Region Science and Technology Support Fund to the research project №16-43-243049.

Albesa-Jové, D., Kariuki, B. M., Kitchin, S. J., Grice, L., Cheung, E. Y. and Harris, K. D. M. (2004). "Challenges in direct-space structure determination from powder diffraction data: a molecular material with four independent molecules in the asymmetric unit," *ChemPhysChem* **5**, 414–418.

Altomare, A., Caliandro, R., Camalli, M., Cuocci, C., Giacovazzo, C., Moliterni, A. G. G. and Rizzi, R. (2004). "Automatic structure determination from powder data with EXPO2004," *J. Appl. Crystallogr.* **37**, 1025–1028.

Andreev, Y. G. and Bruce, P. G. (1988). "Solving crystal structures of molecular solids without single crystals: a simulated annealing approach," *J. Chem. Soc. Dalton Trans.* **24**, 4071–4080.

Andreev, Y. G., Lightfoot, P. and Bruce, P. G. (1997). "A new Monte Carlo approach to structure solution from powder data," *J. Appl. Crystallogr.* **30**, 294–305.

Bevan, D. J. M., Drennan, J. and Rossell, H. J. (1982). "Structure determination of the fluorite-related superstructure phases Er10W2O21 and Y10W2O21," *Acta Crystallogr.* **B38**, 2991–2997.

Burakov, S. V., Zaloga, A. N., Semenkin, E. S. and Yakimov, I. S. (2015). "Research on convergence of multipopulation binary- and real-coded genetic algorithms for solution of crystal structure from X-ray powder diffraction data," *Cryst. Res. Technol.* **50**, 724–728.

Chernyaev, I. I. (1964). *Synthesis of Complex Compounds of Platinum Group Metals. Directory* (Science, Moscow), pp. 160–161.

David, W. I. F., Shankland, K. and Shankland, N. (1998). "Routine determination of molecular crystal structures from powder diffraction data," *Chem. Commun.* **8**, 931–932.

David, W. I. F., Shankland, K., Van de Streek, J., Pidcock, E., Motherwell, W. D. S. and Cole, J. C. (2006). "DASH: a program for crystal structure determination from powder diffraction data," *J. Appl. Crystallogr.* **39**, 910–915.

Falahiazar, L., Teshnehlav, M. and Falahiazar, A. (2012). "Parallel Genetic Algorithm based on a new migration strategy," *Proc. of Int. Conf. on Recent Advances in Computing and Software Systems.* 37–41.

Favre-Nicolin, V. and Černý, R. (2002). "FOX, 'Free Objects for crystallography': a modular approach to ab initio structure determination from powder diffraction," *J. Appl. Crystallogr.* **35**, 734–743.

Feng, Z. J. and Dong, C. (2007). "GEST: a program for structure determination from powder diffraction data using a genetic algorithm," *J. Appl. Crystallogr.* **40**, 583–588.

Griffin, T. A. N., Shankland, K., van de Streek, J. and Cole, J. (2009a). "GDASH: a grid-enabled program for structure solution from powder diffraction data," *J. Appl. Crystallogr.* **42**, 356–359.

Griffin, T. A. N., Shankland, K., van de Streek, J. and Cole, J. (2009b). "MDASH: a multi-core-enabled program for structure solution from powder diffraction data," *J. Appl. Crystallogr.* **42**, 360–361.

Habershon, S., Harris, K. D. M. and Johnston, R. L. (2003). "Development of a multipopulation parallel genetic algorithm for structure solution from powder diffraction data," *J. Comput. Chem.* **24**, 1766–1774.

Harris, K. D. M., Johnston, R. L., and Kariuki, B. M. (1998). "The genetic algorithm: foundations and applications in structure solution from powder diffraction data," *Acta Crystallogr. A, Found. Crystallogr.* **54**, 632–645.

Kariuki, B. M., Zin, D. M. S., Tremayne, M. and Harris, K. D. M. (1996). "Crystal structure solution from powder X-ray diffraction data: the development of Monte Carlo methods to solve the crystal structure of the gamma-phase of 3-chloro-trans-cinnamic acid," *Chem. Mater.* **8**, 565.

Kariuki, B. M., Serrano-González, H., Johnston, R. L. and Harris, K. D. M. (1997). "The application of genetic algorithm for solving crystal structures from powder diffraction data," *Chem. Phys. Lett.* **280**, 189–195.

Kurose, S., Yamamori, K., Aikawa, M. and Yoshihara, I. (2012). "Asynchronous migration for parallel genetic programming on a computer cluster with multi-core processors," *Artif. Life Robot.* **16**, 533–536.

Le Bail, A. and Cranswick, L. M. D. (2009). "Third structure determination by powder diffractometry round robin (SDPDRR-3)," *Powder Diffr.* **24**, 254–262.

Lutterotti, L. and Bortolotti, M. (2003). "Object oriented programming and fast computation techniques in Maud, a program for powder diffraction analysis written in java," *IUCr: Compcomm Newsl.* **1**, 43–50.

Marchand, R., Piffard, Y. and Tournoux, M. (1975). "Structure cristalline de l'orthostannate de potassium K₄SnO₄," *Acta Crystallogr.* **B31**, 511–514.

Martens, K.-P. and Hoppe, R. (1978). "Neue Oxoplumbate(II) A₂PbO₂ (A = K, Rb, Cs) mit zweikernigen Gruppen [OPbO₂PbO]," *Z. Anorg. Allg. Chem.* **440**, 81–104.

Mattausch, H. and Müller-Buschbaum, H. (1974). "Zur Kristallstruktur von Ba₂CrO₄," *Z. Anorg. Allg. Chem.* **407**, 129–134.

Meredig, B. and Wolverton, C. (2013). "A hybrid computational–experimental approach for automated crystal structure solution," *Nat. Mater.* **12**, 123–127.

Nalepa, J. and Blocho, M. (2014). "Co-operation in the Parallel Memetic Algorithm," *Int. J. Parallel Program.* **43**, 1–28.

Ozkan, O., Ermis, M. and Bekmezci, I. (2015). "A hybrid matheuristic approach for designing reliable wireless multimedia sensor networks," *Proc. of the Companion Publication of the 2015 Annual Conf. on Genetic and Evolutionary Computation*, pp. 875–882.

Pennington, W. T. (1999). "DIAMOND – visual crystal structure information system," *J. Appl. Crystallogr.* **32**, 1028–1029.

Rohlíček, J., Hušák, M. and Favre-Nicolin, V. (2010). "Fox.Grid distributed computing," <http://fox.vincefn.net/Manual/Fox.Grid>

Shankland, K., David, W. I. F. and Csoka, T. (1997). "Crystal structure determination from powder diffraction data by the application of a genetic algorithm," *Z. Kristallogr.* **212**, 550–552.

Shankland, K., Spillman, M. J. and Kabova, E. A. (2013). "The principles underlying the use of powder diffraction data in solving pharmaceutical crystal structures," *Acta Crystallogr.* **69**, 1251–1259.

- Solovyov, L. A. (2004). "Full-profile refinement by derivative difference minimization," *J. Appl. Crystallogr.* **37**, 743–749.
- Spek, A. L. (2003). "Single-crystal structure validation with the program PLATON," *J. Appl. Crystallogr.* **36**, 7–13.
- To, C. and Elati, M. (2013). "A parallel Genetic Programming for Single Class Classification," *Proc. of the 15th Annual Conf. Companion on Genetic and Evolutionary Computation*, pp. 1579–1586.
- Whitfield, P. S., Davidson, I. J., Mitchell, L. D., Wilson, S. A. and Mills, S. J. (2010). "Problem solving with the TOPAS macro language: corrections and constraints in simulated annealing and rietveld refinement," *Mater. Sci. Forum* **651**, 11–25.
- Xia, Z., Molokeev, M. S., Oreshonkov, A. S., Atuchin, V. V., Liu, R.-S. and Dong, C. (2014). "Crystal and local structure refinement in $\text{Ca}_2\text{Al}_3\text{O}_6\text{F}$ explored by X-ray diffraction and Raman spectroscopy," *Phys. Chem. Chem. Phys.* **16**, 5952–5957.
- Yakimov, Y. I., Kirik, S. D., Semekin, E. S., Solovyov, L. A. and Yakimov, I. S. (2013). "The evolutionary method of modeling the crystal structure of substances from powder diffraction data," *J. Siber. Fed. Univ., Chem.* **6**, 180–191.
- Zaloga, A. N., Burakov, S. V., Semekin, E. S. and Yakimov, I. S. (2014). "Multi-population genetic algorithm for determination the crystal structure of substances from X-ray diffraction data," *J. Siber. Fed. Univ., Chem.* **7**, 572–580.